10

LINEARIZING VOLTAGE-DEPENDENT CURRENTS

We hinted several times at the fact that a small excitatory synaptic input in the presence of voltage-dependent channels will lead to a local depolarization, followed by a hyperpolarization (Fig. 10.1). Those of us who built our own radios will recognize such an overshooting response as being indicative of so-called RLC circuits which include resistances, capacitances as well as *inductances*. As a reminder, a linear inductance is defined as a circuit element whose instantaneous I–V relationship is,

$$V(t) = -L\frac{dI(t)}{dt} \tag{10.1}$$

where L is the inductance measured in units of henry (abbreviated as H). Although neurobiology does not possess any coils or coillike elements whose voltage is proportional to the current change, membranes with certain types of voltage- and time-dependent conductances can behave as *if* they contained inductances. We talk of a *phenomenological inductance*, a phenomenon first described by Cole (1941) and Cole and Baker (1941) in the squid axon (see Cole, 1972). Under certain circumstances, discussed further below, such damped oscillations can become quite prominent.

This behavior can be obtained in an entirely linear system, as can be observed when reducing (in numerical simulations) the amplitude of the synaptic input (or step current): even though the voltage excursion around steady-state becomes smaller and smaller, the overshoot persists (Fig. 10.1). It is not due to any amplification inherent in such a membrane but is caused by its time- and voltage-dependent nature. Such a linear membrane, whose constitutive elements do not depend on either voltage or time, and which behaves like a bandpass element, has been called *quasi-active* (Koch, 1984) to distinguish it from a truly *active*, that is, nonlinear membrane.

In this chapter, we will explain in considerable detail how an inductance-like behavior can arise from these membranes by linearizing the Hodgkin–Huxley equations. Experimentally, this can be done by considering the *small-signal* response of the squid giant axon and

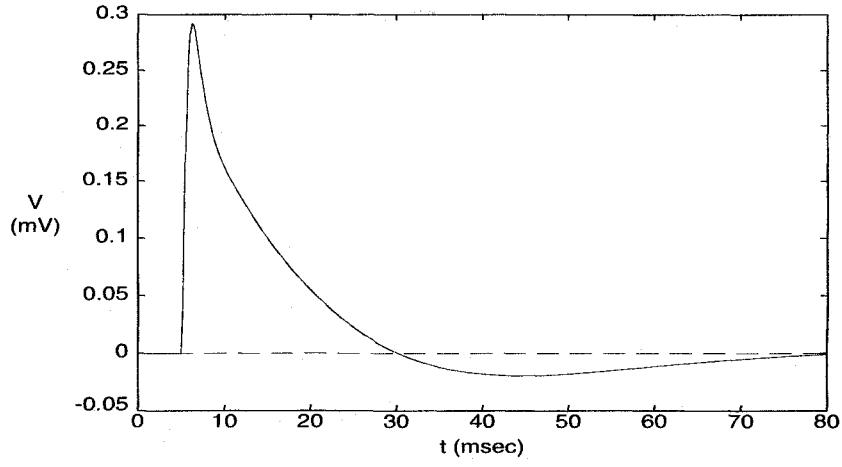

Fig. 10.1 A QUASI-ACTIVE MEMBRANE A small (g_{peak} = 1 nS) excitatory synaptic input close to the soma of a simulated pyramidal cell (Fig. 18.1B) gives rise to an EPSP followed by a small hyperpolarization due to activation of somatic potassium currents. This overshoot is not due to any nonlinearity in the system since it can be observed for arbitrarily small inputs. (If the synaptic input is reduced by a factor of 100 to g_{peak} = 0.01 nS and the associated EPSP rescaled by 100 and superimposed onto the larger amplitude response, the curves cannot be distinguished.) The system behaves like a linear electrical circuit containing an *inductance*-like element and the associated membrane is called *quasi-active*.

comparing it against the theoretical predicted value, a further test of the veracity of the Hodgkin–Huxley equations, which they passed with flying colors. For more details on the linearization procedure we will be using, consult the original references (Chandler, FitzHugh, and Cole, 1962; Sabah and Leibovic, 1969; and the very clear Mauro et al., 1970). Although such a linearization has been applied to membranes other than the squid axon (Clapham and DeFelice, 1976, 1982) we will primarily discuss this well-explored model system.

10.1 Linearization of the Potassium Current

In order to demonstrate the principle behind this linearization, we will describe the procedure in detail for the potassium current of the Hodgkin–Huxley equation (Eq. 6.4 and Fig. 10.2A):

$$I_K = \bar{g}_K n^4 (V - E_K) . \tag{10.2}$$

Let us consider small variations of this current around some fixed potential V_r. We can express such a variation as

$$\delta I_K = \left(\frac{\partial I_K}{\partial V}\right)_r \delta V + \left(\frac{\partial I_K}{\partial n}\right)_r \delta n , \tag{10.3}$$

where both derivatives are evaluated at the potential around which the system is linearized, hence the subscript r. Retaining only the first-order terms and neglecting all higher order ones (such as $(\delta n)^2$ or $\delta n \delta V$) is at the heart of the linearization procedure. We have

$$\left.\frac{\partial I_K}{\partial V}\right|_r = \bar{g}_K n_\infty^4(V_r) = G_K \tag{10.4}$$

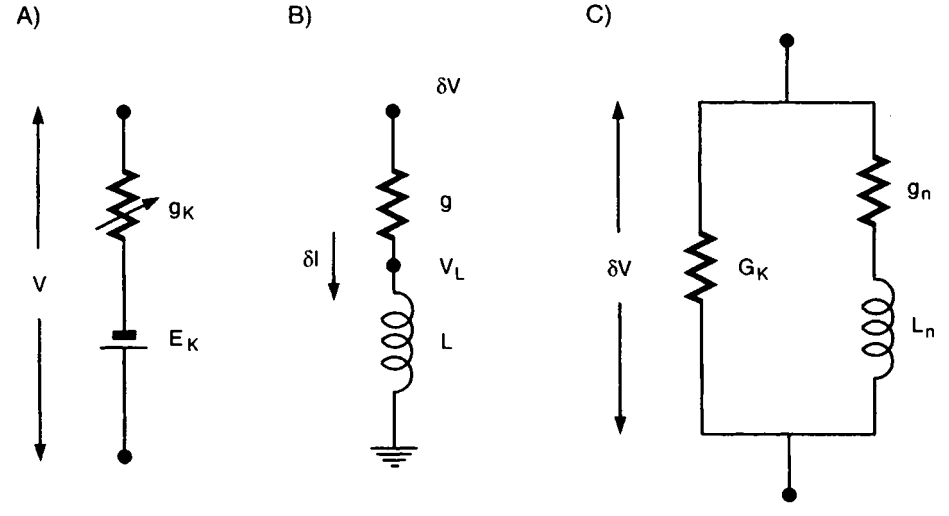

Fig. 10.2 PHENOMENOLOGICAL INDUCTANCE ASSOCIATED WITH THE LINEARIZED POTASSIUM CURRENT **(A)** Equivalent electrical circuit for a noninactivating potassium current. The conductance g_K is given by $\bar{g}_K n^4$, with n the voltage- and time-dependent activation constant. **(B)** Conductance g in series with an inductance L. The voltage across both components is δV and the current through them δI. V_L is the voltage at the intermediate location. **(C)** Equivalent circuit when the potassium current (in panel A) is linearized around some fixed membrane potential. The response to this circuit mimics the small-signal response of the potassium current I_K around some potential V_r. It includes a pure conductance, $G_K = \bar{g}_K n^4$, in parallel with a conductance g_n in series with an inductance L_n. For $V_m > E_K$, all three components are positive.

(see Fig. 10.2C) and

$$\frac{\partial I_K}{\partial n} = 4\bar{g}_K n^3 (V - E_K) . \tag{10.5}$$

We eliminate the variation in the rate constant δn by recalling Eq. 6.6 governing its dynamics,

$$\frac{dn}{dt} = \alpha_n (1 - n) - \beta_n n . \tag{10.6}$$

For small variations we can expand this to

$$\frac{d\delta n}{dt} = \delta\alpha_n - (\delta\alpha_n + \delta\beta_n) n - (\alpha_n + \beta_n)\delta n . \tag{10.7}$$

Since α_n and β_n only depend on the membrane potential, we can express their variations as

$$\delta\alpha_n = \left(\frac{d\alpha_n}{dV}\right) \delta V \tag{10.8}$$

and

$$\delta\beta_n = \left(\frac{d\beta_n}{dV}\right) \delta V . \tag{10.9}$$

Replacing these two expression into Eq. 10.7 leads to

$$\frac{d\delta n}{dt} = \left(\frac{d\alpha_n}{dV}\right) \delta V - (\alpha_n + \beta_n)\delta n - n \left(\frac{d(\alpha_n + \beta_n)}{dV}\right) \delta V . \tag{10.10}$$

This can be formally expressed as

$$\left(\frac{d}{dt} + \alpha_n + \beta_n\right)\delta n = \left[\left(\frac{d\alpha_n}{dV}\right) - n\left(\frac{d(\alpha_n + \beta_n)}{dV}\right)\right]\delta V . \tag{10.11}$$

When replacing this result in Eq. 10.3 and exploiting Eqs. 10.4 and 10.5, we arrive at the following equation for the first-order variation of the potassium current

$$\delta I_K = \left[G_K + \frac{a}{d/dt + b}\right]\delta V , \tag{10.12}$$

with two parameters that need to be evaluated at the membrane potential at which the current is linearized,

$$a = 4\bar{g}_K n^3 (V - E_K)\left[\left(\frac{d\alpha_n}{dV}\right) - n\left(\frac{d(\alpha_n + \beta_n)}{dV}\right)\right] \tag{10.13}$$

and

$$b = \alpha_n + \beta_n . \tag{10.14}$$

In order to understand Eq. 10.12 let us apply Kirchhoff's voltage law to the one branch circuit shown in Fig. 10.2B. With δI the current through both components we can write

$$(\delta V - V_L) + (V_L - 0) = \delta V . \tag{10.15}$$

Eliminating the voltage V_L, we are left with

$$\left(g + L\frac{d}{dt}\right)\delta I = \delta V . \tag{10.16}$$

Comparing this result with the second component on the right-hand side of Eq. 10.12 we can see that they are very similar. Indeed, the voltage δV across the electrical circuit with two branches drawn in Fig. 10.2C is the same as δV in Eq. 10.12 if

$$g_n = \frac{a}{b} = \frac{4\bar{g}_K n^3 (V - E_K)\left[(d\alpha_n/dV)_r - n\,(d(\alpha_n + \beta_n)/dV)_r\right]}{\alpha_n + \beta_n} \tag{10.17}$$

and if we set the inductance to

$$L_n = \frac{1}{a} = \frac{1}{g_n(\alpha_n + \beta_n)} . \tag{10.18}$$

For a small perturbation δV around V_r, the potassium current responds as though the conductance G_K (in units of S·cm^2) is shunted by the conductance g_n (also in S·cm^2) in series with the inductance L_n (in units of sec·cm^2/S, that is, in H·cm^2). By examining the slopes of the on and off rates α_n and β_n (Eqs. 6.10 and 6.11), we see that for the entire range of relevant voltages, $V \geq E_K$, all three electrical components are always positive.

Mauro et al., (1970) captured the key point of the previous analysis in a graphical manner; see Fig. 10.3. As before, we assume that we are only considering the small-signal response (this is, after all, what any linearization procedure amounts to) of the potassium current around some fixed potential V_r (positive to E_K). Injecting a current step $I_{inj} > 0$ at this potential will turn on the potassium current I_K (Fig. 10.3A). Because the underlying potassium conductance requires some time to increase to its final value, the initial change in membrane potential δV is given by the injected current divided by the conductance G_K. In the absence of any capacitance, this causes the membrane to depolarize instantaneously

by I_{inj}/G_K, moving in the direction of the dotted slope (the vector labeled $\mathbf{t}_0$ in Fig. 10.3A). However, this depolarization will eventually led to an increase in the potassium conductance, which causes the voltage change δV to *decrease* with time, as indicated by the trajectory in Fig. 10.3C, to finally approach the new steady-state value of the membrane potential V_r, (around $\mathbf{t}_2$). In other words, as expected of an inductance—inducing a voltage proportional to the change in current—δV rises instantaneously and then falls off gradually. This analysis also makes obvious the fact that this inductive behavior is caused by both the time and the voltage dependency of the membrane conductance.

When the current I_{inj} terminates, the inverse occurs (Fig. 10.3B). δV first undershoots V_r, relaxing with a time lag back to its earlier steady-state value V_r. The response is inductive for both on and off steps (provided that $V_r > E_K$). If the capacitive nature of the neuronal membrane is included, the phenomenological inductance combines with the capacitance to give a damped oscillatory response (Fig. 10.3C).

10.2 Linearization of the Sodium Current

In a similar manner, we can compute the small-signal response of the sodium current,

$$I_{Na} = \bar{g}_{Na} m^3 h (V - E_{Na}) . \tag{10.19}$$

By taking variations and retaining only the first-order terms we arrive at

$$\delta I_{Na} = \left(\frac{\partial I_{Na}}{\partial V}\right)_r \delta V + \left(\frac{\partial I_{Na}}{\partial m}\right)_r \delta m + \left(\frac{\partial I_{Na}}{\partial h}\right)_r \delta h \tag{10.20}$$

that is,

$$\delta I_{Na} = \bar{g}_{Na} m^3 h \delta V + 3\bar{g}_{Na} m^2 h (V - E_{Na}) \delta m + \bar{g}_{Na} m^3 (V - E_{Na}) \delta h . \tag{10.21}$$

Following the same procedure to eliminate the variational variables δm and δh as for the potassium current leaves us with an equation for the small-signal change in the sodium current:

$$\delta I_{Na} = G_{Na} \delta V + \frac{g_m(\alpha_m + \beta_m)}{d/dt + \alpha_m + \beta_m} \delta V + \frac{g_h(\alpha_h + \beta_h)}{d/dt + \alpha_h + \beta_h} \delta V \tag{10.22}$$

with

$$G_{Na} = \bar{g}_{Na} m^3 h \tag{10.23}$$

$$g_m = \frac{3\bar{g}_{Na} m^2 h (V - E_{Na}) \left[(d\alpha_m/dV)_r - m \left(d(\alpha_m + \beta_m)/dV \right)_r \right]}{\alpha_m + \beta_m} \tag{10.24}$$

and

$$g_h = \frac{\bar{g}_{Na} m^3 (V - E_{Na}) \left[(d\alpha_h/dV)_r - h(d(\alpha_h + \beta_h)/dV)_r \right]}{\alpha_h + \beta_h} \tag{10.25}$$

all evaluated at $V = V_r$. As illustrated in Fig. 10.4A, this describes the current flow in a three-branch electrical circuit with inductances

$$L_m = \frac{1}{g_m(\alpha_m + \beta_m)} \tag{10.26}$$

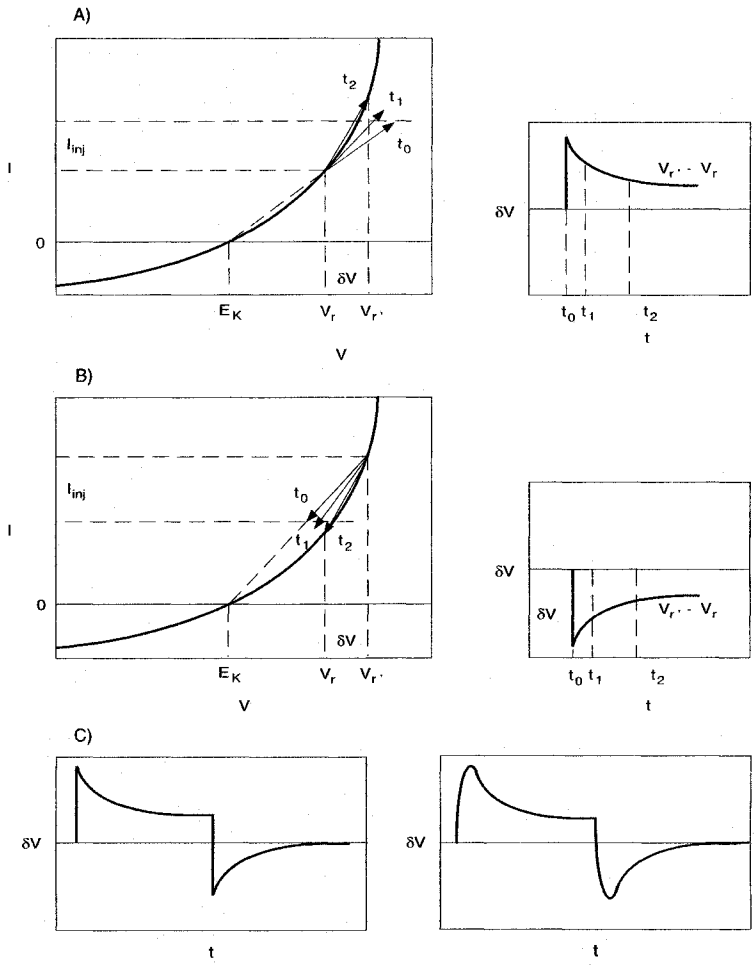

Fig. 10.3 Graphical Interpretation of the Linearization Procedure Following the lead of Mauro et al., (1970), we here illustrate the linearization procedure for the potassium current I_K. **(A)** Steady-state I–V relationship of a potassium current is indicated schematically and we are considering the small-signal response around the potential V_r. Not shown is the time dependency of the underlying potassium conductance. Injecting a positive current I_{inj} leads to an instantaneous jump of the membrane potential to a new value (which lies along the dotted line going through the reversal potential E_K) given by I_{inj}/G_K (the vector labeled t_0). As the potassium conductance gradually adapts to its new value and increases, the voltage change δV becomes smaller, until it converges to its new value V_r' (from t_0 to t_1 to t_2; left panel). This inductive behavior would not be evident in a stationary nonlinear membrane. **(B)** Upon termination of the current step I_{inj}, the voltage change δV first overshoots before settling to its old value. **(C)** Complete voltage response to the current injection in the absence of any membrane capacitance (left panel). When the capacitance is added to the circuit, a damped oscillatory response results (right panel).

and

$$L_h = \frac{1}{g_h(\alpha_m + \beta_m)} . \tag{10.27}$$

The two inductive branches reflect the separate contributions from the activating and the inactivating components of the sodium conductance.

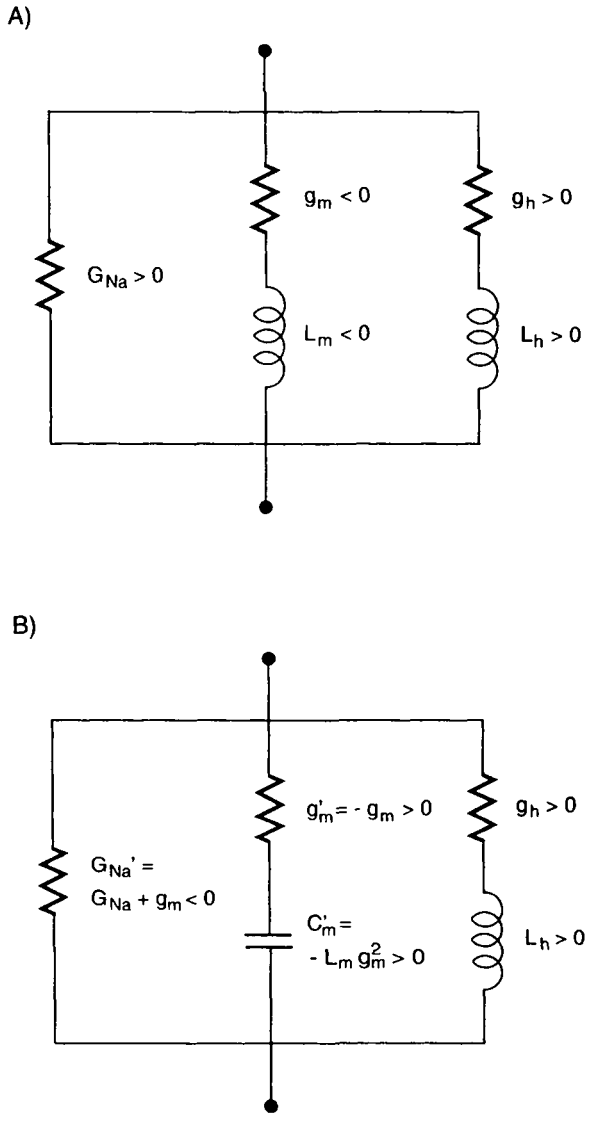

Fig. 10.4 ***RLC*** **CIRCUIT FOR THE LINEARIZED SODIUM CURRENT** **(A)** Electrical *RLC* circuit obtained by linearizing the Hodgkin-Huxley sodium current at some potential below E_{Na}. Both elements associated with the activation variable are negative. **(B)** These negative elements can be transformed into a positive conductance g'_m in series with a positive phenomenological capacitance C'_m, with a shunt conductance G'_{Na} that is negative.

At this point, a problem arises. For the voltage range of interest, that is, $E_K \leq V \leq E_{Na}$, the resistive and inductive components of the inactivating branch of the circuit, that is, g_h and L_h, are positive, but the corresponding circuit elements of the m branch are negative: $g_m < 0$ and, therefore, $L_m < 0$. The negative conductance arises as a consequence of the negative slope of the I_{Na}–V curve.

We can fix this problem by transforming the negative components into an equivalent RC system (Fig. 10.4B) with

$$G'_{\mathrm{Na}} = G_{\mathrm{Na}} + g_m \tag{10.28}$$

$$g'_m = -g_m \tag{10.29}$$

and a positive capacitance, instead of a negative inductance,

$$C'_m = -L_m \cdot g_m^2 . \tag{10.30}$$

This capacitance is also a phenomenological one, in the sense that activating the sodium current leads to similar behavior (for small perturbation) as would the existence of an additional capacitive branch.

For $V < E_{\mathrm{Na}}$, the conductance g'_m and the capacitance C'_m are positive, but the shunting conductance G'_{Na} is negative. This is to be expected if we only treat I_{Na} in isolation, with no counteracting current. Indeed, in order for the circuit to be stable, the total steady-state conductance must be positive (Koch, 1984). This can be assured if the linearized potassium current as well as the leak current are all jointly considered, as we will do now.

10.3 Linearized Membrane Impedance of a Patch of Squid Axon

The final RLC circuit, mimicking the small-signal response of a patch of squid axon membrane, includes five branches (Fig. 10.5A): a pure capacitance due to the physical capacitance of the bilipid membrane, a single positive conductance lumping the steady-state contributions of the leak, sodium, and potassium currents, the two phenomenological inductive branches and the one phenomenological capacitive branch. The values of these electrical elements vary with V_r, as discussed in Mauro et al., (1970) and in the legend to Fig. 10.5.

We know from electrical circuit theory that RLC circuits can show oscillatory behavior with the presence of one or more resonances. This is best investigated by computing the complex impedance $\tilde{K}(f)$ of the circuit in Fig. 10.5A. Writing down an expression for the total current (see Eqs. 10.12 and 10.22) directly in Fourier space, we have

$$\delta\tilde{V}(f) = \tilde{K}(f) \cdot \left(\delta\tilde{I}_{\mathrm{K}}(f) + \delta\tilde{I}_{\mathrm{Na}}(f) + \delta\tilde{I}_{\mathrm{leak}}(f)\right) . \tag{10.31}$$

With $d\delta I(t)/dt$ transforming into $if \cdot \delta\tilde{I}(f)$, we obtain an expression for the impedance as the ratio of $\delta\tilde{V}(f)$ and $\delta\tilde{I}(f)$:

$$\tilde{K}(f) = \frac{\beta_3(if)^3 + \beta_2(if)^2 + \beta_1(if) + \beta_0}{\alpha_4(if)^4 + \alpha_3(if)^3 + \alpha_2(if)^2 + \alpha_1(if) + \alpha_0} . \tag{10.32}$$

The α_i's and β_i's are constants, which depend on the values of the electrical components (Koch, 1984). Figure 10.5B shows the calculated amplitude of the impedance if the membrane is linearized around the resting potential, and Fig. 10.5C shows the experimentally recorded amplitude. Both sets of curves have the same characteristic bandpass response. For the low-temperature curves, sinusoidal inputs in the neighborhood of 50–70 Hz are more attenuated than slower or more rapidly varying current inputs. The linearized squid axon membrane behaves similar to a passive membrane for sinusoidal inputs with 200 Hz or faster components.

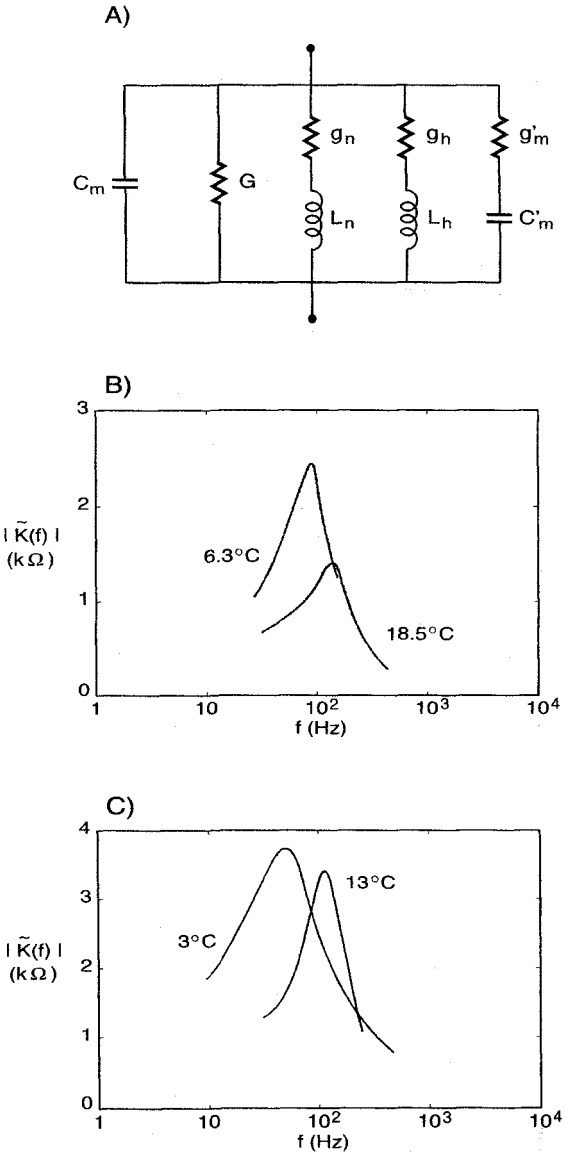

Fig. 10.5 Linearized Squid Axon Membrane **(A)** Electrical RLC circuit mimicking the small-signal response of a patch of squid axon obtained by adding δI_K, δI_{Na}, as well as the contribution from the leak current δI_{leak}. Note that G is positive. If the Hodgkin–Huxley equations with standard parameters (at 6.3° C; see Chap. 6) are linearized around rest, the following numerical values are obtained (for details, see the appendix in Koch, 1984): $C_m = 1$, $G = 0.246$, $g_n = 0.849$, $g_h = 0.072$, $g'_m = 0.432$, $L_n = 6.43$, $L_h = 119.0$ and $C'_m = 0.102$ (units are $\mu F/cm^2$ for the capacitances, $H \cdot cm^2$ for the inductances, and mS/cm^2 for the conductances). The combined steady-state conductance of the system at rest is 1.167 mS/cm^2. **(B)** Amplitude of the membrane impedance of this circuit, corresponding to the impedance of the small-signal response of the squid axon at two different temperatures. As expected of a *quasi-active* membrane, the transversal membrane impedance displays a resonance around 67 Hz. Reprinted in modified form by permission from Mauro et al., (1970). **(C)** Amplitude of the small-signal impedance measured in the space-clamped squid axon at two different temperatures. Reprinted in modified form by permission from Mauro et al., (1970).

The range of validity of the linearized membrane is a few millivolts around the resting potential (for more details, see Sabah and Leibovic, 1969; Koch, 1984). This is evident in the experimental record from the squid axon displayed in Fig. 10.6A. Here, a current step of increasing magnitude is injected into the space-clamped squid giant axon (see Fig. 6.2A for the experimental arrangement). As is apparent, the voltage has a characteristic ringing response as well as displaying undershooting at the offset of the current step. This ringing becomes more pronounced for larger, but still subthreshold, current stimuli, revealing nonlinear components. A similar experiment is repeated in Fig. 10.6B, where an action potential is elicited at the top of the oscillation.

It makes sense to associate a *resonant frequency* with the membrane impedance, defined

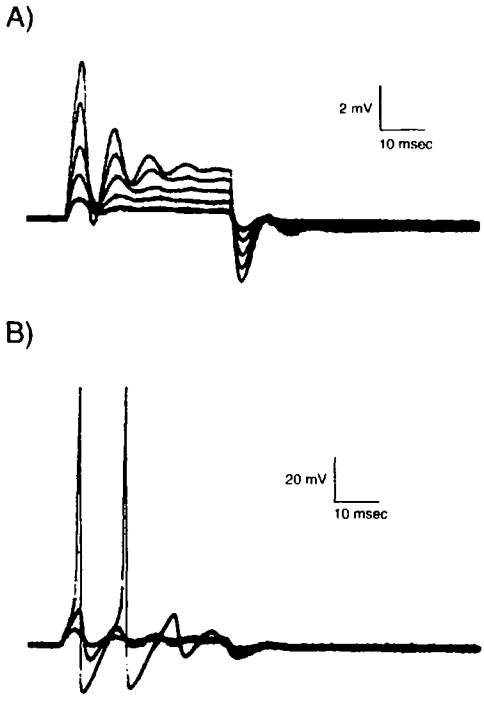

Fig. 10.6 Small-Signal Voltage Response in Squid Axon Membrane potential in a space-clamped giant axonal fiber (of 0.4-mm diameter). **(A)** Membrane potential in response to depolarizing current steps of different amplitudes. Notice the damped oscillations during and at the offset of the current step. The maximum current strength applied is barely subthreshold in the last case. Reprinted in modified form by permission from Mauro et al., (1970). **(B)** A suprathreshold current of sufficient amplitude is applied to evoke a second action potential that arises from the second oscillation. At higher current amplitudes, a train of spikes can be generated with a moderate increase in repetition rate relative to the subthreshold oscillation frequency. Reprinted in modified form by permission from Mauro et al., (1970).

here as the frequency of the peak response of $\tilde{K}(f)$. If the standard Hodgkin–Huxley equations at 6.3° C are linearized around rest, $f_{max} = 67$ Hz (Fig. 10.6B). This frequency is relatively stable for larger current steps, as is evident in Fig. 10.5B, varying no more than 15% and roughly coinciding with the frequency of the oscillatory components seen in the experimental records. Furthermore, f_{max} is only marginally higher than the natural spiking frequency of an "infinite" train of action potentials (53 Hz; see Fig. 6.9B).

So far, we only considered a patch of squid membrane (or, equivalently, a space-clamped axon). On the basis of the propagation factor $\gamma(f)$ defined in Sec. 2.3.1, the input and transfer impedances as well as the frequency-dependent space constant of the linearized squid axon can be computed. It is possible to prove (Koch, 1984) that if the membrane impedance is a bandpass, then so will these three functions for an infinite cable. For instance, a 1 μm thin infinite cable with the quasi-active membrane shown in Fig. 10.5A has a dc space constant of 175 μm. In any passive cable structure, the space constant at higher frequency will always be less than the dc space constant (Fig. 2.8), due to the unavoidable charge leakage via the membrane capacitance. While this capacitance is also present, the inductances "present" in the linearized squid axon can boost $\lambda(f)$ for an intermediate frequency range (for the definition of the frequency-dependent space constant in an infinite cable see Eq. 2.36). Thus, $\lambda(f)$ has a pronounced peak (345 μm) at 74 Hz. The sharpness of the tuning curve (as expressed by its half width at half height) as well as the resonant frequency f_{max} increase monotonically with the channel density of both potassium and sodium channels as well as with the distance between the injection and the recording sites (Koch, 1984).

Figure 10.7A shows the computed amplitude of the somatic input impedance of our standard model of the layer 5 pyramidal cell as a function of the frequency of the applied sinusoidal current injection. While its dendritic tree is passive, the soma contains seven

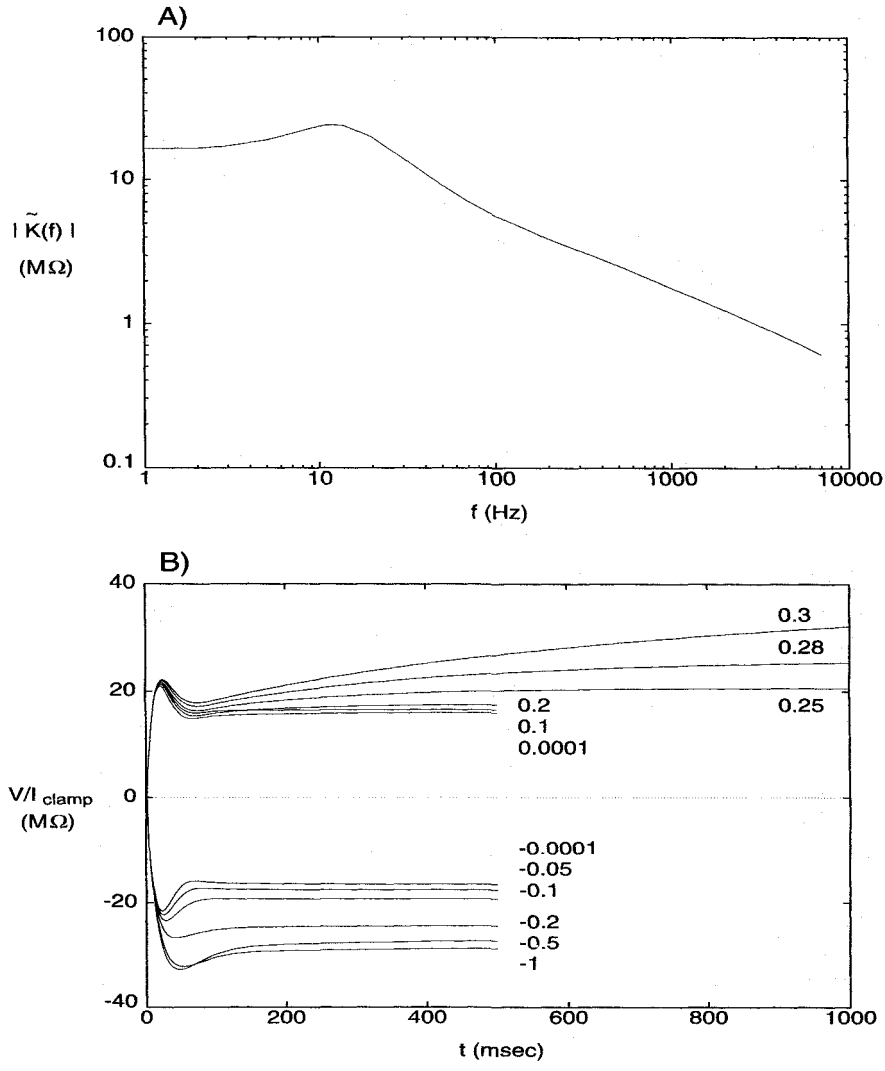

Fig. 10.7 SMALL-SIGNAL SOMATIC INPUT IMPEDANCE OF PYRAMIDAL CELL MODEL Small-signal response of the voltage-dependent model of the layer 5 pyramidal cell. **(A)** Amplitude of the somatic input impedance $|\tilde{K}_{ss}(f)|$ defined as the peak somatic voltage change relative to the resting potential (at −65 mV) in response to a small sinusoidal current (peak amplitude of 10 pA) of frequency f injected into the soma. The peak occurs around 12 Hz. The roll-off at high frequency is due to the distributed capacitance. **(B)** The range of this linear approximation is illustrated by plotting the normalized membrane change in response to current steps I_{clamp}. For currents less then 0.1 nA, the responses superimpose and the depolarizing response is a mirror image of the hyperpolarizing response. Larger currents increasingly deviate from this linear behavior. For current steps of 0.30 nA, the membrane potential slowly drifts upward, eventually initiating an action potential.

voltage-, time-, and calcium-dependent membrane conductances. $\tilde{K}$ is computed using a small-signal response. The amplitude of $\tilde{K}$ is 16.5 MΩ at dc and peaks at 24.1 MΩ around 12 Hz. At these frequencies, the transient potassium current I_A is relatively inactivated (the inactivation rate constant has a time constant of 100 msec). The decay evident at high

frequencies is due to the membrane capacitance and has a dependency close to $1/\sqrt{f}$, as expected in an infinite cable. (At these high frequencies, the neuron can be considered to have a practical infinite extent relative to $\lambda(f)$; Fig. 2.9.) The range of validity of this small-signal approximation to the neuronal response can be directly read off Fig. 10.7B. For current steps up to 0.1 nA, this relatively large cell is in its linear range. Larger currents, in particular if they are depolarizing, will trigger a sufficient amount of sodium current to bring the cell out of its linear range. For a step of 0.295 nA amplitude, the potential will slowly creep upward until an action potential is initiated (not shown; see Sec. 17.3).

10.4 Functional Implications of Quasi-Active Membranes

What are some of the computational implications for neurons with quasi-active membranes? The fact that the input and transfer impedances and the frequency-dependent space constant have peaks at nonzero frequencies has interesting consequences for information processing. Let us allude to three examples.

10.4.1 Spatio-Temporal Filtering

In a dendritic tree endowed with a purely passive membrane, $\tilde{K}_{ij}$ and λ are monotonically decreasing functions of the frequency of the applied current. As illustrated with the help of the dynamic morphoelectrotonic transforms in Fig. 3.8, voltage attenuation is substantially more pronounced at higher than at lower frequencies. For a neuron in the visual pathway, say in the retina, this effect will partly determine its receptive field, since a visual stimulus with a high frequency content can only influence the cell's firing if it is closer to the cell body than more slowly varying synaptic input of the same amplitude. This effect is caricaturized in Fig. 10.8A. In a sort of precursor to METs, Koch (1984) determined the fraction of the dendritic tree of a cat retinal ganglion cell whose voltage attenuation to the soma, A_{is}, for two different frequencies is less than 4. This amounts to a functional definition of the *receptive field* of the cell (assuming that the synaptic inervation density is constant across its dendrites). If the dendritic tree is entirely passive, the "receptive field" of this cell is large for dc synaptic input, shrinking to a much smaller size for 100 Hz input.

If, to the contrary, the cell is endowed with the quasi-active membrane shown in Fig. 10.5A, the opposite behavior occurs. Because the membrane impedance is higher for high-frequency inputs, the fraction of the dendritic tree for which $A_{is} \leq 4$ is large for 100 Hz input, and small for either dc or 200 Hz input (Fig. 10.8B). Assuming that the processing between the photoreceptor and the ganglion cell is linear for low-contrast visual stimuli, this neuron would be tuned to transient input and would respond less to sustained stimuli, a form of spatio-temporal tuning (Derrington and Lennie, 1982; Enroth-Cugell et al., 1983).

10.4.2 Temporal Differentiation

Computing the temporal derivative of some function $V(t)$ is equivalent to multiplying its Fourier transform $\tilde{V}(f)$ by if. Such a differentiation operation can be implemented by filtering $V(t)$ with a function whose Fourier transform is proportional to f.

While the transfer impedance of any neuronal membrane will ultimately decay with increasing frequency (due to the presence of the capacitance), the transfer impedance in a cable endowed with a quasi-active membrane shows a high-pass behavior over a limited

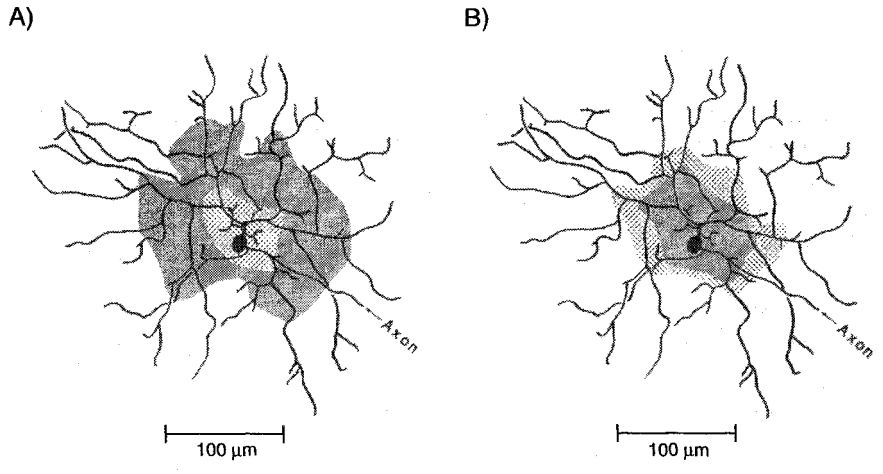

Fig. 10.8 SPATIO-TEMPORAL FILTERING IN RETINAL GANGLION CELLS In a cell endowed with a quasi-active membrane, high-frequency synaptic input can propagate further than sustained input. This effect is shown here graphically by determining the fraction of the dendritic tree whose voltage attenuation to the soma is less than some threshold, here $A_{is} \leq 4$ in a cat retinal ganglion cell reconstructed from Boycott and Wässle (1974). This can be thought of as the receptive field of the cell. **(A)** The membrane is entirely passive. The large, heavily dotted area indicates the region within which the voltage attenuation for stationary inputs to the soma is less than 4. The smaller, lightly dotted area illustrates the same concept for a sinusoidal input of 100 Hz. **(B)** If the quasi-active membrane obtained from the linearized Hodgkin–Huxley equations (Fig. 10.5A) is added to the passive component in panel A, the previous situation is reversed. Now a sinusoidal current input at 100 Hz (lightly dotted region) attenuates much less than sustained input (heavily dotted region). For 200-Hz input the region of small attenuation will be less than for the region for sustained input. Such a cell would be more responsive to transient than to dc signals. Reprinted by permission from Koch (1984).

frequency range. If the signal is restricted to this part of the spectrum, then such a membrane can implement a temporal derivative operation.

Koch (1984) simulated this behavior in an extended, unbranched cable with the quasi-active membrane of Fig. 10.5A. Injecting a current that peaks at 5 msec and decays within 20 msec (whose spectrum is monotonically decreasing and has decayed to 50% of its dc value at 70 Hz, the peak frequency of the transfer) the voltage recorded 350 μm away is qualitatively very similar to the temporal derivative of the current injected into the cable. The approximation is worse for faster synaptic input (since a larger fraction of its spectrum will lie beyond the peak at $f_{\max}$) and better for slowly changing input. What is appealing about this linear operation is that it can be implemented in a very compact manner in a single cable.

10.4.3 Electrical Tuning in Hair Cells

Receptor cells in auditory and electroreceptive systems of many species show *electrical resonance*: upon appropriate sensory stimulation, their membrane potential oscillates. This has been explored in detail for hair cells in the amphibian auditory system. *Hair cells*, whose function is to translate the acoustic stimuli into electrical ones (for an incisive review of their biophysical properties, see Hudspeth, 1985), are organized tonotopically along the basilar membrane in the cochlea according to their characteristic frequency (the frequency

of the acoustic stimuli the cell optimally responds to). Upon stimulation with a current step, the membrane potential responds with exponentially damped oscillations (Crawford and Fettiplace, 1981; Lewis and Hudspeth, 1983; see Fig. 10.9A). The oscillation frequency is a nonlinear function of the membrane potential. The frequency around the resting potential indicates the cell's natural frequency, that is, the frequency of sound or vibration to which the cell is most sensitive. In the bullfrog, this ranges from 80 to 160 Hz and in the turtle from 100 to about 700 Hz.

Hudspeth and Lewis (1988a,b) used the patch-clamp technique to identify the biophysical mechanism responsible for this resonance. They characterized two key currents, a noninactivating calcium current I_{Ca}, and a calcium- and voltage-dependent potassium current $I_{K(Ca)}$ (which they modeled using a linear, five-state kinetic scheme that requires two intracellular Ca^{2+} ions for the channel to open, and a third Ca^{2+} ion that can prolong the channel opening; Hudspeth and Lewis, 1988a). Using a Hodgkin–Huxley-like model, which also incorporates the capacitive and leak currents, they showed that electrical tuning could be explained in its majority by the interdependence of these currents (Hudspeth and Lewis, 1988b). Injection of a step current depolarizes the membrane, activating I_{Ca}. Calcium ions rush in and rapidly turn on $I_{K(Ca)}$. This outward current then brings the membrane potential down again, turning itself off in the process. If the current step persists, the cycle can now begin anew. Varying the kinetics and the density of the calcium-dependent calcium channels controls the frequency of resonance.

The input to hair cells is provided by activation of the mechanically sensitive cilia (hairs) that modulate a conductance in their membrane. If this conductance is included in the model and stimulated using sinusoidally varying acoustical input, the resulting tuning curve (Fig. 10.9B) closely mimics the electrical resonance frequency around the resting potential. We conclude that in the amphibian cochlea, hair cells behave like small electrical resonant elements—bandpass filters— whose tuning properties are due to the interplay of an inward and an outward current. Note that Hudspeth and Lewis (1988b) used a nonlinear model to explain the electrical resonance. Previous efforts to model hair cells using *RLC* circuits as described above (Crawford and Fettiplace, 1981; Art and Fettiplace, 1987) did, however, capture most of the qualitative aspects of these oscillations.

Have such resonating neuronal elements been found anywhere else? Llinás, Grace, and Yarom (1991), recording in layer 4 neurons in the cortical slice preparation, found that a constant current step evoked subthreshold oscillations in the 10–50 Hz frequency range. Because these cells are small, with smooth and aspiny dendrites, Llinás and coworkers argue that they are inhibitory interneurons. In contradistinction, other neurons in the cortex, termed *chattering cells*, show an oscillatory firing pattern in the 20–70 Hz band in response to visual stimuli or suprathreshold current injection, but no such oscillatory changes in the membrane potential in response to subthreshold current injections (Gray and McCormick, 1996). The function of these oscillations is at present not known, although much has been speculated on this topic (for an overview, see Koch, 1993).

10.5 Recapitulation

Although it can be argued that a linear analysis of a nonlinear phenomenon does not do justice to it, it will certainly help us to understand certain aspects of the mechanism underlying the phenomenon. This is true when considering certain resonant or oscillatory behaviors evident in nerve cells.

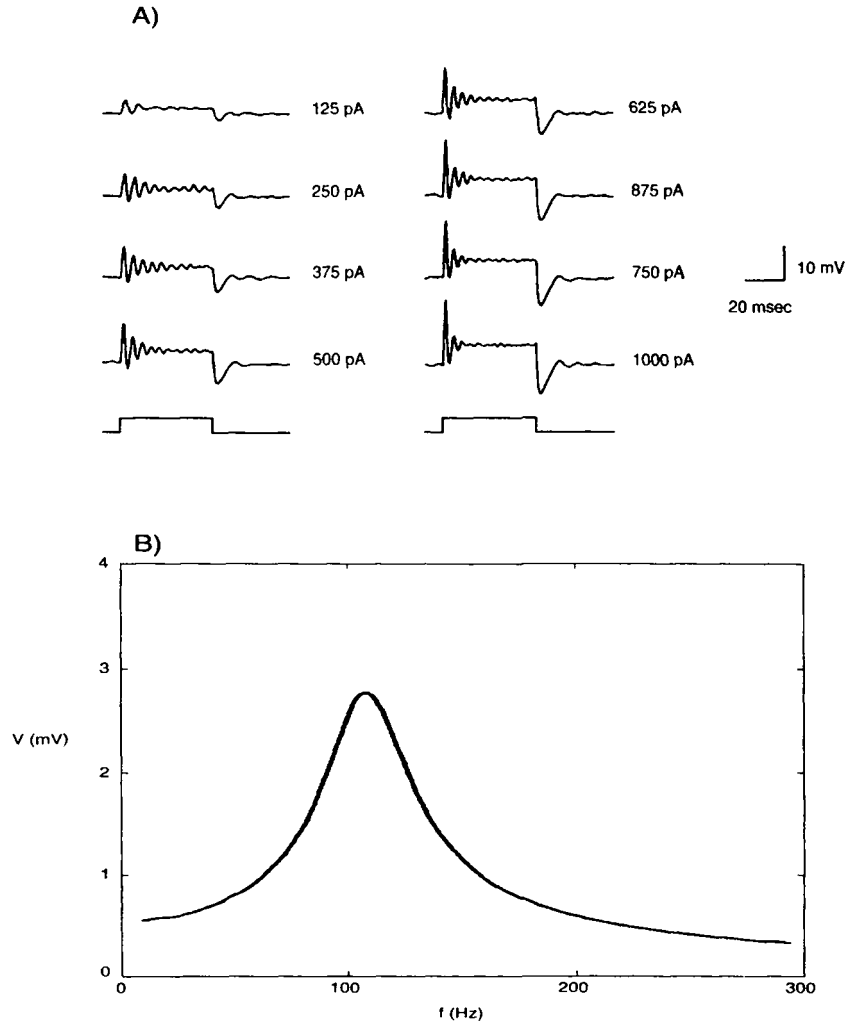

Fig. 10.9 Electrical Resonance in Hair Cells Hair cells in the cochlea of amphibians behave like electrical band-pass elements, preferentially responding to an acoustic stimulus of a particular frequency. **(A)** Membrane potential recorded in a solitary hair cell of the bullfrog (Hudspeth and Lewis, 1988b). Upon injection of a 50-msec-long current step, the membrane responds by generating exponentially damped oscillations whose frequency varies with the membrane potential. The frequency (93 Hz) around the resting potential (−49 mV) determines the frequency of sound or vibration the cell is most sensitive to. As the average membrane potential increases to −41 mV (by using larger current steps, whose amplitude is indicated to the right of each trace), the frequency of the damped oscillations increases to 240 Hz. Reprinted by permission from Hudspeth and Lewis (1988b). **(B)** The acoustic stimulus couples to a mechanically triggered membrane conductance. If this conductance is added to a model that includes a calcium and a calcium-dependent potassium current, it is sufficient to explain the resonant property of isolated hair cells. Here the peak-to-peak amplitude of the receptor potential in response to a sinusoidal ±20-nm displacement of the hair bundle is plotted as a function of the stimulus frequency. Thus, each individual cell acts like a bandpass element, here optimally sensitive to input around 112 Hz. Reprinted by permission from Hudspeth and Lewis (1988b).

As Detwiler, Hodgkin and McNaughton (1980) pointed out, a time- and voltage-dependent potassium current that is activated by depolarization or an inward current that is activated by hyperpolarization (as the h part of the fast sodium current) does behave, under certain restricted conditions, like an inductance in series with a conductance would. That is, one can mimic the small-signal behavior of such a current by an electrical circuit that includes such an inductance. This explains why EPSPs or the depolarization in response to even very small current injections will be followed by a hyperpolarizing overshoot (provided the experimental setup is sensitive enough to record such small voltages superimposed onto the background noise). The membrane impedance of a membrane that includes resistances, capacitances, as well as phenomenological inductances (RLC circuit) peaks at some nonzero resonant frequency f_{max}. Such a quasi-active membrane with a bandpass response will cause the membrane potential to show damped oscillations at or close to the resonant frequency f_{max} in response to a current step. This has been confirmed empirically when recording the response of the squid giant axon to small, subthreshold current steps.

One consequence of a bandpass-like membrane impedance is that the transfer impedance and the frequency-dependent space constant associated with an infinite cable covered by such a quasi-active membrane can also show resonant behavior. This implies that input signals with frequencies around f_{max} are treated preferentially in terms of a smaller voltage attenuation to the soma (or other measures of synaptic efficiency) than inputs at faster or slower frequencies: the cable is spatio-temporally tuned to some frequency range. If the transfer impedance of a cable with a quasi-active membrane can be approximated by a bandpass, injecting a current whose dominant signal content lies in the spectrum between dc and f_{max} induces a voltage change that approximates the continuous temporal derivative of the injected current. In other words, a small piece of quasi-active dendritic cable can implement a temporal derivative operation.

Hudspeth and Lewis (1988b) used a nonlinear, squid axonlike membrane description of a calcium and a calcium-dependent potassium current (in series with leak and capacitive currents) to model the electrical behavior of bullfrog hair cells in the cochlea. Confirming earlier linear RLC analyses, each hair cell by itself acts as an electrical resonant element best tuned to respond to sounds in the f_{max} frequency band. The kinetics and density of $I_{K(Ca)}$ control f_{max} as well as the tuning of the bandpass. The morale is that individual neurons can implement a variety of different linear and nonlinear computational operations on the basis of the cornucopia of known membrane currents.